their regulatory protein. In addition to inhibitory phosphorylation of PP1, it should be noted that NIPP1 is also subject to regulation by phosphorylation, decreasing its association with PP1 (39, 40).

Interestingly, NIPP1-ΔC promoted severe splicing defects *in vivo* but not *in vitro*. Although *in vitro* splicing assays are reliable and widely used, they may not always reflect *in vivo* conditions, at least in terms of PP1. In fact, some investigators have reported differences between *in vivo* and *in vitro* splicing. For example, a sub-domain of U2AF65, an essential splicing factor, plays important role *in vivo* but not *in vitro* (41).

In summary, our results provide evidence that NIPP1 directs PP1 to dephosphorylate Sap155. Further elucidation of the role of the NIPP1 C terminus in regulating PP1 and identification of specific Sap155 sites dephosphorylated by PP1 will be required to fully understand how pre-mRNA splicing is regulated by protein phosphorylation/dephosphorylation cycles. Also, cell lines conditionally expressing NIPP1-ΔC, which mediates a decrease in Sap155 hyperphosphorylation, will be useful to analyze the roles of Sap155 phosphorylation.

Acknowledgments—We acknowledge Dr. H. Brahms and Dr. R. Lührmann (Max-Planck Institute, Göttingen, Germany) for kindly providing the anti-U5-116k antibody, and Dr. S. Ohno (Yokohama City University, Japan) for the pTRE-BGG plasmid (referred to as pTRE-β-globin in this paper). We also thank E. Yoshida for secretarial assistance.

REFERENCES

1. Misteli, T. (1999) *Curr. Biol.* **9,** R198–R200
2. Hastings, M. L., and Krainer, A. R. (2001) *Curr. Opin. Cell Biol.* **13,** 302–309
3. Stamm, S. (2008) *J. Biol. Chem.* **283,** 1223–1227
4. Wang, C., Chua, K., Seghezzi, W., Lees, E., Gozani, O., and Reed, R. (1998) *Genes Dev.* **12,** 1409–1414
5. Bessonov, S., Anokhina, M., Will, C. L., Urlaub, H., and Lührmann, R. (2008) *Nature* **452,** 746–750
6. Shi, Y., Reddy, B., and Manley, J. L. (2006). *Mol. Cell* **23,** 819–829
7. Ceulemans, H., and Bollen, M. (2004) *Physiol. Rev.* **84,** 1–39
8. Eto, M., Senba, S., Morita, F., and Yazawa, M. (1997) *FEBS Lett.* **410,** 356–360
9. Greengard, P. (2001). *Science* **294,** 1024–1030
10. Weiser, D. C., Sikes, S., Li, S., and Shenolikar, S. (2004) *J. Biol. Chem.* **279,** 48904–48914
11. Dohadwala, M., da Cruz e Silva, E. F., Hall, F. L., Williams, R. T., Carbonaro-Hall, D. A., Nairn, A. C., Greengard, P., and Berndt, N. (1994) *Proc. Natl. Acad. Sci. U. S. A.* **91,** 6408–6412
12. Yamano, H., Ishii, K., and Yanagida, M. (1994) *EMBO J.* **13,** 5310–5318
13. Berndt, N., Dohadwala, M., and Liu, C. W. (1997) *Curr. Biol.* **7,** 375–386
14. Liu, C. W., Wang, R. H., Dohadwala, M., Schönthal, A. H., Villa-Moruzzi, E., and Berndt, N. (1999) *J. Biol. Chem.* **274,** 29470–29475
15. Van Eynde, A., Nuytten, M., Dewerchin, M., Schoonjans, L., Keppens, S., Beullens, M., Moons, L., Carmeliet, P., Stalmans, W., and Bollen, M. (2004) *Mol. Cell. Biol.* **24,** 5863–5874
16. Egloff, M. P. F., Johnson, D., Moorhead, G., Cohen, P. T., Cohen, P., and Barford, D. (1997) *EMBO J.* **16,** 1876–1887
17. Beullens, M., Vulsteke, V., Van Eynde, A., Jagiello, I., Stalmans, W., and Bollen, M. (2000) *Biochem. J.* **352,** 651–658
18. Boudrez, A., Beullens, M., Groenen, P., Van Eynde, A., Vulsteke, V., Jagiello, I., Murray, M., Krainer, A. R., Stalmans, W., and Bollen, M. (2000) *J. Biol. Chem.* **275,** 25411–25417
19. Boudrez, A., Beullens, M., Waelkens, E., Stalmans, W., and Bollen, M. (2002) *J. Biol. Chem.* **277,** 31834–31841
20. Vulsteke, V., Beullens, M., Boudrez, A., Keppens, S., Van Eynde, A., Rider, M. H., Stalmans, W., and Bollen, M. (2004) *J. Biol. Chem.* **279,** 8642–8647
21. Durocher, D., Taylor, I. A., Sarbassova, D., Haire, L. F., Westcott, S. L., Jackson, S. P., Smerdon, S. J., and Yaffe, M. B. (2000) *Mol. Cell* **6,** 1169–1182
22. Kumeta, H., Ogura, K., Adachi, S., Fujioka, Y., Tanuma, N., Kikuchi, K., and Inagaki, F. (2008) *J. Biomol. NMR* **40,** 219–224
23. Beullens, M., and Bollen, M. (2002) *J. Biol. Chem.* **277,** 19855–19860
24. Trinkle-Mulcahy, L., Ajuh, P., Prescott, A., Claverie-Martin, F., Cohen, S., Lamond, A. I., and Cohen, P. (1999) *J. Cell Sci.* **112,** 157–168
25. Achsel, T., Ahrens, K., Brahms, H., Teigelkamp, S., and Lührmann, R. (1998) *Mol. Cell. Biol.* **18,** 6756–6766
26. Isono, K., Mizutani-Koseki, Y., Komori, T., Schmidt-Zachmann, M. S., and Koseki, H. (2005) *Genes Dev.* **19,** 536–541
27. Takizawa, N., Mizuno, Y., Ito, Y., and Kikuchi, K. (1994) *J. Biochem. (Tokyo)* **116,** 411–415
28. Yamashita, A., Ohnishi, T., Kashima, I., Taya, Y., and Ohno, S. (2001) *Genes Dev.* **15,** 2215–2228
29. Kim, S. E., Ishita, A., Shima, H., Nakamura, K., Yamada, Y., Ogawa, K., and Kikuchi, K. (2000) *Int. J. Oncol.* **16,** 751–755
30. Mitsuhashi, S., Shima, H., Tanuma, N., Matsuura, N., Takekawa, M., Urano, T., Kataoka, T., Ubukata, M., and Kikuchi, K. (2003) *J. Biol. Chem.* **278,** 82–88
31. Niranjanakumari, S., Lasda, E., Brazas, R., and Garcia-Blanco, M. A. (2002) *Methods (San Diego)* **26,** 182–190
32. Maniatis, T., and Reed, R. (2002) *Nature* **416,** 499–506
33. Friend, K., Lovejoy, A. F., and Steitz, J. A. (2007) *Mol. Cell* **28,** 240–252
34. Tran, H. T., Ulke, A., Morrice, N., Johannes, C. J., and Moorhead, G. B. (2004) *Mol. Cell. Proteomics* **3,** 257–265
35. Johnson, D., Cohen, P., Chen, M. X., Chen, Y. H., and Cohen, P. T. W. (1997) *Eur. J. Biochem.* **244,** 931–939
36. Seghezzi, W., Chua, K., Shanahan, F., Gozani, O., Reed, R., and Lees, E. (1998) *Mol. Cell. Biol.* **18,** 4526–4536
37. de Graaf, K., Czajkowska, H., Rottmann, S., Packman, L. C., Lilischkis, R., Luscher, B., and Becker, W. (2006) *BMC Biochem.* **7,** 7
38. Massiello, A., Roesser, J. R., and Chalfant, C. E. (2006) *FASEB J.* **20,** 1680–1682
39. Beullens, M., Van Eynde, A., Bollen, M., and Stalmans, W. (1993) *J. Biol. Chem.* **268,** 13172–13177
40. Van Eynde, A., Beullens, M., Stalmans, W., and Bollen, M. (1994) *Biochem. J.* **297,** 447–449
41. Banerjee, H., Rahn, A., Gawande, B., Guth, S., Valcarcel, J., and Singh, R. (2004) *RNA (N. Y.)* **10,** 240–253

nature genetics

FGF9 monomer–dimer equilibrium regulates extracellular matrix affinity and tissue diffusion

Masayo Harada[1,2], Hirotaka Murakami[3,11], Akihiko Okawa[3,11], Noriaki Okimoto[4,11], Shuichi Hiraoka[1,10,11], Taka Nakahara[5,10,11], Ryogo Akasaka[6,11], Yo-ichi Shiraishi[7,11], Noriyuki Futatsugi[4], Yoko Mizutani-Koseki[1], Atsushi Kuroiwa[7], Mikako Shirouzu[6], Shigeyuki Yokoyama[6,8], Makoto Taiji[4], Sachiko Iseki[5], David M Ornitz[9] & Haruhiko Koseki[1]

The spontaneous dominant mouse mutant, Elbow knee synostosis (*Eks*), shows elbow and knee joint synosotsis, and premature fusion of cranial sutures. Here we identify a missense mutation in the *Fgf9* gene that is responsible for the *Eks* mutation. Through investigation of the pathogenic mechanisms of joint and suture synostosis in *Eks* mice, we identify a key molecular mechanism that regulates FGF9 signaling in developing tissues. We show that the *Eks* mutation prevents homodimerization of the FGF9 protein and that monomeric FGF9 binds to heparin with a lower affinity than dimeric FGF9. These biochemical defects result in increased diffusion of the altered FGF9 protein ($FGF9^{Eks}$) through developing tissues, leading to ectopic FGF9 signaling and repression of joint and suture development. We propose a mechanism in which the range of FGF9 signaling in developing tissues is limited by its ability to homodimerize and its affinity for extracellular matrix heparan sulfate proteoglycans.

The fibroblast growth factors (FGFs) are widely expressed in developing and adult tissues and have diverse functions in organogenesis, tissue repair, nervous system control, metabolism and physiological homeostasis[1]. In humans and mice, the 22 FGF ligands are expressed in a spatiotemporally regulated manner and mediate signals through seven different isoforms of FGF receptors (FGFRs)[1]. The pharmacologic potential of FGF ligands has been highlighted by identification of gain-of-function mutations in genes encoding FGFRs 1–3 in individuals with chondrodysplasia and craniosynostosis syndromes[2,3]. These human diseases identify essential roles of FGF signaling not only in development but also in homeostasis of bones and joints.

Given these clinical, genetic and biochemical studies in humans and mice, the coordinated development of bones and joints seems to rely on precise FGFR signaling. This suggests that spatiotemporal constraints on FGF signaling are a prerequisite for appropriate functions *in vivo* and are indeed modulated at several distinct levels. First, the expression of FGF ligands is spatiotemporally restricted. Among the 22 FGF ligands, FGF2, FGF4, FGF7, FGF8, FGF9, FGF10, FGF17 and FGF18 are expressed in the limb bud and developing skeleton[4–6]. Of these, loss-of-function mutations have demonstrated that FGF2, FGF9 and FGF18 are involved in chondrogenesis and/or osteogenesis[7–10]. Induction of chondrodysplastic phenotypes by overexpression of FGF9 in mice also shows its ability to affect chondrogenesis[11]. Other elements implicated in FGF signaling are the heparan sulfate proteoglycans (HSPGs). Genetic studies in mice and *Drosophila melanogaster* suggest that HSPGs regulate the distribution and receptor binding of FGF ligands[12,13]. Finally, structural analyses of FGF9 suggest that it may form homodimers that could affect its ability to signal[14,15]. Because FGF9 homodimerization occludes several critical receptor binding sites, an autoinhibitory mechanism may function to modulate FGF9-dependent signal transduction. However, a functional demonstration of this proposed mechanism is lacking.

We have previously reported that a dominant mouse mutant, Elbow knee synostosis (*Eks*), shows radiohumeral and tibiofemoral synostosis, craniosynostosis (**Supplementary Fig. 1** online) and lung hypoplasia[16]. In this study, we identify a missense mutation that replaces Asn143 with threonine in the *Fgf9* gene in *Eks* mutant mice. We designate this mutant allele as $Fgf9^{Eks}$ and show that this mutation

[1]RIKEN Research Center for Allergy and Immunology, 1-7-22 Suehiro-cho, Tsurumi-ku, Yokohama, Kanagawa 230-0045, Japan. [2]Department of Immunology and [3]Department of Orthopaedic Surgery, Graduate School of Medicine, Chiba University, 1-8-1 Inohana, Chuo-ku, Chiba 260-8670, Japan. [4]RIKEN Advanced Science Institute, Computational Systems Biology Research Group, 61-1 Ono-cho, Tsurumi-ku, Yokohama, Kanagawa 230-0046, Japan. [5]Section of Molecular Craniofacial Embryology, Graduate School of Medical and Dental Sciences, Tokyo Medical and Dental University, 1-5-45 Yushima, Bunkyo-ku, Tokyo 113-8549, Japan. [6]RIKEN Systems and Structural Biology Center, 1-7-22 Suehiro-cho, Tsurumi-ku, Yokohama, Kanagawa 230-0045, Japan. [7]Division of Biological Science, Graduate School of Science, Nagoya University, Furo-cho, Chikusa-ku, Nagoya 464-8602, Japan. [8]Department of Biophysics and Biochemistry, Graduate School of Science, The University of Tokyo, 7-3-1 Hongo, Bunkyo-ku, Tokyo 113-0033, Japan. [9]Department of Developmental Biology, Washington University School of Medicine, 660 South Euclid Avenue, St. Louis, Missouri 63110, USA. [10]Present addresses: Department of Systems Biomedicine, National Research Institute for Child Health and Development, 2-10-1 Okura, Setagaya-ku, Tokyo 157-8535, Japan (S.H.) and Section of Developmental and Regenerative Dentistry, School of Life Dentistry at Tokyo, The Nippon Dental University, 1-9-20 Fujimi, Chiyoda-ku, Tokyo 102-8159, Japan (T.N.). [11]These authors contributed equally to this work. Correspondence should be addressed to H.K. (koseki@rcai.riken.jp).

Received 20 June 2008; accepted 22 December 2008; published online 15 February 2009; doi:10.1038/ng.316

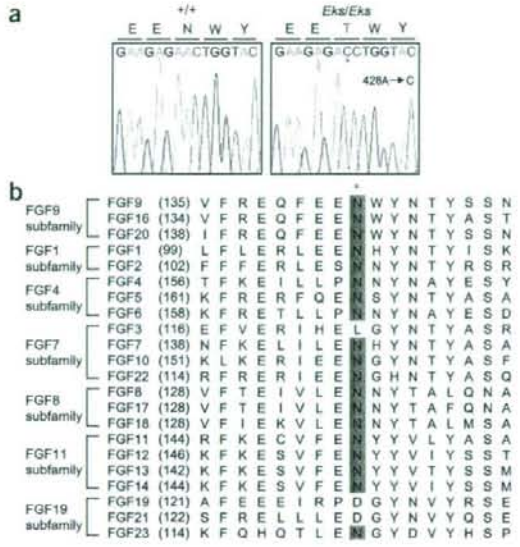

Figure 1 Missense mutation in the *Fgf9* gene of *Eks* mice. (**a**) Nucleotide sequence of the *Fgf9* cDNA derived from +/+ and *Eks/Eks* mice. *Eks* mutants have an A-to-C substitution at position 428, which results in the replacement of Asn143 with threonine. The *Eks* missense mutation is indicated by the asterisk, and the corresponding amino acid is shown in purple. (**b**) Structure-based sequence alignment of human FGFs. The amino acid sequence surrounding the N143T substitution in $FGF9^{Eks}$ and that of its corresponding domain in other human FGF family proteins are aligned on the basis of sequence identity. The Asn143 residue in FGF9 is highly conserved among most FGF proteins (purple box). The asterisk denotes the site of *Eks* mutation.

prevents homodimerization of FGF9, consequently decreasing the affinity of FGF9 for heparin. As a result, $FGF9^{Eks}$ is more diffusible in developing tissues, leading to ectopic FGF9 signaling in the prospective joints and sutures where it functions to repress development. Molecular-dynamics calculations suggest that the reduction in FGF9 affinity for heparin is due to the predominance of the monomeric form rather than to changes in its intrinsic affinity for heparin. We thus propose a mechanism in which the range of FGF9 signaling in developing tissues is limited through regulation of its affinity for HSPGs, which is at least in part controlled by the FGF9 monomer–dimer equilibrium. These observations could have far-reaching implications for the pharmacologic manipulation of FGF signaling under a variety of circumstances and in a wide range of tissues.

RESULTS

Eks is caused by a missense mutation in *Fgf9*

The *Eks* mutation was mapped between the polymorphic markers *D14Mit62* and *D14Mit5* on mouse chromosome 14 (ref. 16). Among 169 genes located in this interval, *Fgf9* seemed a likely candidate for the *Eks* mutation because FGF9 is a ligand for FGFR2c and FGFR3c[17] and is expressed in the developing limbs, cranial sutures and developing lung[8,18,19]. Sequence analysis of *Fgf9* cDNA from homozygous *Eks* mice revealed an A-to-C substitution at position 428, which resulted in the replacement of Asn143 with threonine (**Fig. 1a**). Notably, the Asn143 residue in FGF9 is highly conserved among most FGF proteins (**Fig. 1b**) and is predicted to be a critical amino acid residue for homodimerization and receptor binding[14,15].

We used a genetic approach to determine whether the N143T substitution in *Fgf9* was responsible for the *Eks* phenotype. We observed a mendelian pattern of inheritance of the mutation among 976 offspring of *Eks* heterozygous ($Fgf9^{Eks/+}$) matings, with heterozygous mice showing mild skeletal phenotypes and homozygous $Fgf9^{Eks/Eks}$ littermates showing severe skeletal phenotypes. The *Eks* phenotype and the mutation in *Fgf9* cosegregated in all cases. The absence of recombination between *Eks* and *Fgf9* among nearly 2,000 meiotic events provides strong evidence that the *Eks* mutation is allelic with *Fgf9*.

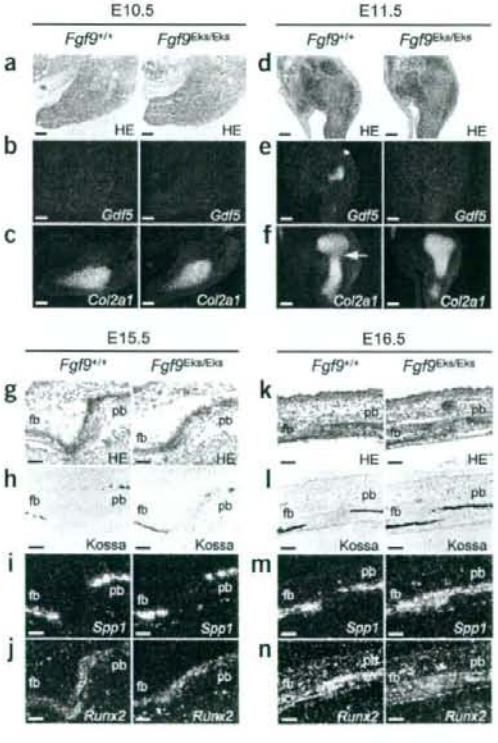

Figure 2 Synostotic phenotypes in $Fgf9^{Eks/Eks}$ mice. (**a–f**) Defects in early specification of prospective elbow joints in $Fgf9^{Eks/Eks}$ embryos. Hematoxylin and eosin staining (**a**,**d**) and *in situ* detection of *Gdf5* (**b**,**e**) and *Col2a1* (**c**,**f**) in the forelimb buds of $Fgf9^{+/+}$ and $Fgf9^{Eks/Eks}$ embryos at E10.5 and E11.5. In $Fgf9^{+/+}$ embryos, there was *Gdf5* expression at the prospective elbow joint (**e**, left), which was demarcated as the gap of *Col2a1* expression (**f**, arrow), at E11.5. In $Fgf9^{Eks/Eks}$ embryos, there was not *Gdf5* expression at the prospective elbow joint (**e**, right). Scale bars, 100 μm. (**g–n**) Ectopic osteogenesis at the coronal sutures in $Fgf9^{Eks/Eks}$ fetuses. Hematoxylin and eosin staining (**g**,**k**) and von Kossa staining (**h**,**l**) and *in situ* detection of *Spp1* (**i**,**m**) and *Runx2* (**j**,**n**) in the coronal suture of $Fgf9^{+/+}$ and $Fgf9^{Eks/Eks}$ fetuses at E15.5 and E16.5. Note the ectopic ossification in the suture of $Fgf9^{Eks/Eks}$ at E16.5. fb, frontal bone; pb, parietal bone. Scale bars, 100 μm.

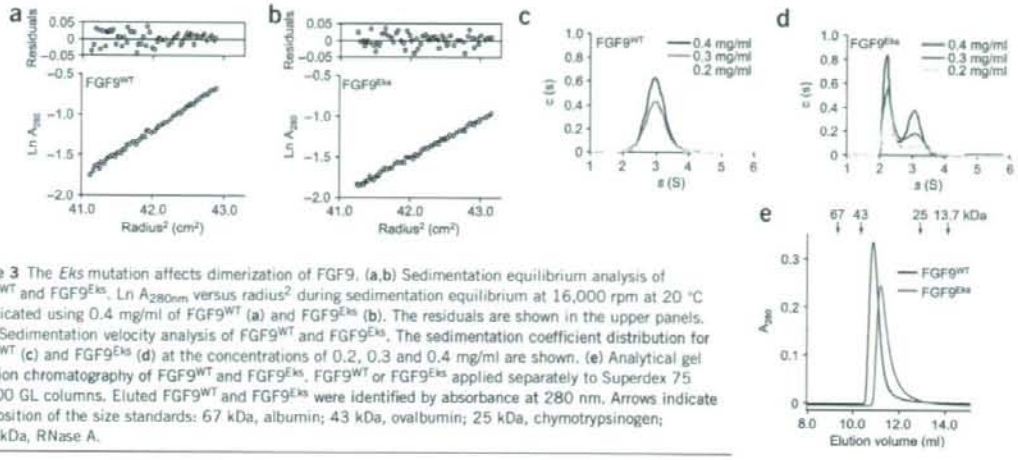

Figure 3 The *Eks* mutation affects dimerization of FGF9. (**a**,**b**) Sedimentation equilibrium analysis of $FGF9^{WT}$ and $FGF9^{Eks}$. Ln A_{280nm} versus radius^2 during sedimentation equilibrium at 16,000 rpm at 20 °C is indicated using 0.4 mg/ml of $FGF9^{WT}$ (**a**) and $FGF9^{Eks}$ (**b**). The residuals are shown in the upper panels. (**c**,**d**) Sedimentation velocity analysis of $FGF9^{WT}$ and $FGF9^{Eks}$. The sedimentation coefficient distribution for $FGF9^{WT}$ (**c**) and $FGF9^{Eks}$ (**d**) at the concentrations of 0.2, 0.3 and 0.4 mg/ml are shown. (**e**) Analytical gel filtration chromatography of $FGF9^{WT}$ and $FGF9^{Eks}$. $FGF9^{WT}$ or $FGF9^{Eks}$ applied separately to Superdex 75 10/300 GL columns. Eluted $FGF9^{WT}$ and $FGF9^{Eks}$ were identified by absorbance at 280 nm. Arrows indicate the position of the size standards: 67 kDa, albumin; 43 kDa, ovalbumin; 25 kDa, chymotrypsinogen; 13.7 kDa, RNase A.

Fgf9$^{Eks/Eks}$ mice phenocopy *Fgfr* gain-of-function mutants

Eks is a dominant mutation and joint synostosis and premature fusion of sutures have also been reported in mice expressing gain-of-function alleles of *Fgfr1* (ref. 20) and *Fgfr2c* (*Fgfr2*^{C342Y})[21]. Furthermore, homozygous *Fgf9* null mutants (*Fgf9*$^{-/-}$) show rhizomelia but not joint or suture synostosis[8]. Thus, we hypothesized that *Fgf9*^{Eks} encodes a gain-of-function mutation. To test this possibility, we first investigated whether there were phenotypic similarities between *Eks* mutants and gain-of-function mutants for *Fgfr1* and *Fgfr2*^{C342Y}. As initiation of elbow joint development was primarily impaired in *Fgfr1* gain-of-function transgenic mice[20], we examined radiohumeral joint development in *Fgf9*$^{Eks/Eks}$ mice (**Fig. 2a–f**). *Gdf5* (ref. 22) and *Col2a1* (ref. 23) demarcate the prospective elbow joint and cartilaginous condensation, respectively. *Gdf5* expression in the prospective joint space was observed as early as embryonic day E11.5 in *Fgf9*$^{+/+}$ control mice, but was completely absent in *Fgf9*$^{Eks/Eks}$ mice (**Fig. 2e**). Analysis of the prospective cartilage revealed a gap of *Col2a1* expression at the prospective elbow joint in E11.5 wild-type embryos (**Fig. 2f**, left). The gap of *Col2a1* expression was absent in *Fgf9*$^{Eks/Eks}$ mice (**Fig. 2f**, right). In summary, ectopic chondrocyte differentiation in the prospective elbow joint of *Fgf9*$^{Eks/Eks}$ mice seems very similar to that seen in transgenic mice that ectopically express an activated *Fgfr1* kinase domain in the presumptive joint field[20].

Premature fusion of coronal sutures in *Fgfr2*^{C342Y} mice results from excess osteogenic differentiation within the coronal suture mesenchyme[21]. To determine whether *Fgf9*$^{Eks/Eks}$ mice had similar histological features, we examined mineralization and the expression of the early osteoblast differentiation markers *Spp1* (ref. 24) and *Runx2* (ref. 25) in the coronal suture (**Fig. 2g–n**). At E15.5, both wild-type and *Fgf9*$^{Eks/Eks}$ mice showed similar coronal suture histology (**Fig. 2g–j**). However, at E16.5 von Kossa staining revealed considerably more overlap of the frontal and parietal bones in *Fgf9*$^{Eks/Eks}$ mice compared to *Fgf9*$^{+/+}$ mice (**Fig. 2l**). *Spp1* expression domains, which demarcate preosteoblasts and osteoblasts, showed wide separation of the frontal and parietal bones in *Fgf9*$^{+/+}$ mice; however, there was overlap in the *Fgf9*$^{Eks/Eks}$ mice (**Fig. 2m**). *Runx2* is highly expressed in immature osteoblasts at the leading edge of the frontal and parietal bones in *Fgf9*$^{+/+}$ mice (**Fig. 2n**, left). In E16.5 *Fgf9*$^{Eks/Eks}$ mice, the intensity of *Runx2* expression in the coronal suture was lower than in *Fgf9*$^{+/+}$ mice (**Fig. 2n**, right), suggesting premature differentiation of the osteoblasts at the presumptive suture. These phenotypes reflect abnormal osteogenic differentiation within the coronal suture mesenchyme and indicate that the defect in suture development occurs before E16.5. Taken together, these observations suggest that the $FGF9^{Eks}$ altered protein mediates excess FGFR signals within the prospective joints and sutures, preventing joint formation and promoting the fusion of cranial sutures.

The *Eks* mutation impairs homodimerization of FGF9

The predicted involvement of the Asn143 residue in homodimerization and receptor activation[14,15] suggests that changes in these processes may account for the apparent gain-of-function activity of the $FGF9^{Eks}$ altered protein. Homodimerization of FGF9 has been proposed to occlude receptor binding sites and consequently mediate an autoinhibitory mechanism for FGF9 signaling. We thus hypothesized that the *Eks* mutation might impair the autoinhibition. To test this possibility, we compared the degree of homodimerization of wild-type ($FGF9^{WT}$) and $FGF9^{Eks}$ proteins by analytical ultracentrifugation. $FGF9^{WT}$ and $FGF9^{Eks}$ were expressed in *Escherichia coli* and purified by column chromatography (**Supplementary Methods** and **Supplementary Fig. 2** online).

The molecular mass and association constant of $FGF9^{WT}$ and $FGF9^{Eks}$ were determined by sedimentation equilibrium centrifugation using the purified recombinant proteins (**Fig. 3a**,**b**). The estimated average molecular masses of $FGF9^{WT}$ and $FGF9^{Eks}$ were 39,264 and 32,929 Da, respectively, whereas the calculated monomeric molecular masses were 20,090 and 20,077 Da, respectively. These data suggest that $FGF9^{WT}$ primarily exists as a dimer, whereas $FGF9^{Eks}$ exists in a monomer–dimer equilibrium. The calculated association constants of $FGF9^{WT}$ and $FGF9^{Eks}$ were 10.4 μM^{-1} and 0.119 μM^{-1}, respectively. We further measured the sedimentation coefficient of $FGF9^{Eks}$ by sedimentation velocity centrifugation. The overlay plots of c(s)-sedimentation coefficient distributions show that $FGF9^{WT}$ has a unimodal peak at 3.0 S for a single ideal species, whereas $FGF9^{Eks}$ has bimodal peaks (2.2 S and 3.1 S) for two ideal species (**Fig. 3c**,**d**). This observation suggests that $FGF9^{WT}$ is present primarily as a dimer, whereas $FGF9^{Eks}$ exists primarily as a monomer. These interpretations are consistent with the retarded elution of $FGF9^{Eks}$

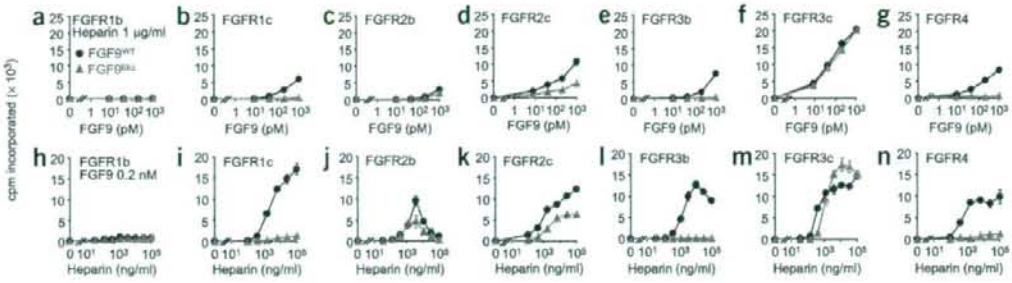

Figure 4 The *Eks* mutation affects the mitogenic activity of FGF9. (**a–g**) Dose-dependent changes in mitogenic activity of $FGF9^{WT}$ and $FGF9^{Eks}$. BaF3 cells expressing exogenous FGFR1b, 1c, 2b, 2c, 3b, 3c or 4 were treated with increasing concentrations of $FGF9^{WT}$ or $FGF9^{Eks}$ in the presence of 1 μg/ml heparin. Cell proliferation was determined by [^{3}H]thymidine incorporation after 36 h in culture. (**h–n**) Heparin-dependent changes in mitogenic activity of $FGF9^{WT}$ and $FGF9^{Eks}$. BaF3 cells expressing the respective FGFR were treated with increasing concentrations of heparin in the presence of 0.2 nM $FGF9^{WT}$ or $FGF9^{Eks}$. Cell proliferation was determined as above. Data are represented as mean ± s.e.m. of triplicate assays. These results are representative of at least two independent experiments.

relative to $FGF9^{WT}$ on a gel filtration column (**Fig. 3e**). Therefore, $FGF9^{Eks}$ is defective in homodimer formation.

$FGF9^{Eks}$ mediates less potent signaling via several FGFRs

To examine whether the *Eks* mutaion altered the binding of FGF9 to FGFRs by impairing the autoinhibitory mechanisms, we compared the ability of $FGF9^{WT}$ and $FGF9^{Eks}$ to activate FGFRs by assaying the mitogenic activity of both proteins on BaF3 cells expressing individual FGF receptors[17]. FGFR-expressing BaF3 cell lines were treated with increasing concentrations of purified recombinant FGF9 in the presence of 1 μg/ml heparin. Compared to $FGF9^{WT}$, $FGF9^{Eks}$ showed less activity on cells expressing any of the FGFRs except FGFR3c, where $FGF9^{Eks}$ showed equivalent activity (**Fig. 4a–g**). To test the ability of heparin to enhance FGF9 activity, we treated the BaF3 cell lines with increasing concentrations of heparin in the presence of 0.2 nM $FGF9^{WT}$ or $FGF9^{Eks}$. $FGF9^{Eks}$ also showed a decreased heparin-dependent mitotic response on all FGFRs except FGFR3c, where $FGF9^{Eks}$ showed higher activity in the presence of high concentrations of heparin (**Fig. 4h–n**). Because $FGF9^{Eks}$ does not mediate excess signaling via FGFRs, other properties of the altered protein must be responsible for the phenotype of the *Eks* mice.

The *Eks* mutation lowers FGF9 affinity for heparin

The decreased heparin-dependent mitogenic activity of $FGF9^{Eks}$ suggested that its affinity for heparin may be reduced. Heparin is functionally very similar to heparan sulfate, which is present in most tissues in the form of HSPGs. HSPGs function to modulate FGFR activation directly, by mediating FGF–FGFR interactions, and indirectly, by binding FGF ligands and regulating their diffusion through the extracellular matrix and thus their access to distant FGFRs[1,12,13,26]. As the gain-of-function property of $FGF9^{Eks}$ may not involve direct interaction with the FGFRs, we hypothesized that its decreased affinity for heparin might allow increased diffusion and thus bioavailability in

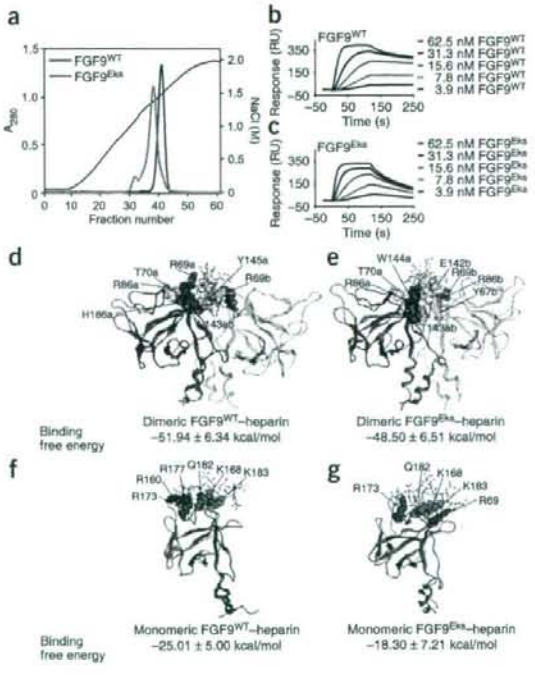

Figure 5 The *Eks* mutation reduces FGF9 affinity for heparin by impairing its dimerization. (**a**) Chromatographic analysis of the affinities of $FGF9^{WT}$ and $FGF9^{Eks}$ for heparin. $FGF9^{WT}$ or $FGF9^{Eks}$ were loaded onto a heparin-conjugated agarose column and eluted with a linear gradient of NaCl from 120 mM to 2.0 M (black line). Elution profiles of $FGF9^{WT}$ and $FGF9^{Eks}$ were determined by monitoring absorbance at 280 nm. (**b,c**) Surface plasmon resonance analysis of the affinities of $FGF9^{WT}$ and $FGF9^{Eks}$ for heparin. Sensorgrams indicating the interaction of $FGF9^{WT}$ (**b**) and $FGF9^{Eks}$ (**c**) with immobilized heparin were determined at different concentrations. The biosensor chip response is indicated on the *y* axis (RU) as a function of time (*x* axis) at room temperature. (**d–g**) The most probable solution structures of dimeric $FGF9^{WT}$–heparin (**d**), dimeric $FGF9^{Eks}$–heparin (**e**), monomeric $FGF9^{WT}$–heparin (**f**) and monomeric $FGF9^{Eks}$–heparin (**g**) complexes deduced by molecular-dynamics simulations. Heparin and protein residues that form important hydrogen bonds are drawn in ball and stick and space-filling modes. The single-letter amino acid code, residue number and chain code are indicated for each of these residues. Computed binding free energy of each complex is shown under the respective illustrated structure. Data are represented as mean ± s.d. of energies obtained from 200 molecular-dynamics snapshots in respective molecular-dynamics trajectory.

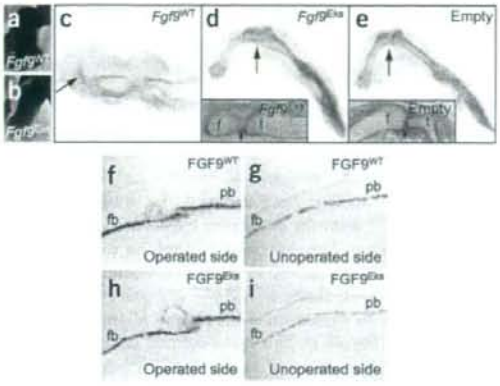

Figure 6 $FGF9^{Eks}$ can inhibit joint and suture development as well as $FGF9^{WT}$. (**a–e**) Inhibition of knee joint development induced by ectopic expression of $Fgf9^{WT}$ and $Fgf9^{Eks}$. Hindlimb buds of Hamburger-Hamilton stage 17 chickens were infected with RCAS-$Fgf9^{WT}$, RCAS-$Fgf9^{Eks}$ or empty RCAS virus. (**a**,**b**) *Fgf9* expression was examined by *in situ* hybridization 2 d after infection. (**c–e**) Respective knee joints (arrows) were examined by Alcian blue staining and hematoxylin and eosin staining of sections through the knee joint (insets in **d** and **e**) 5 d after infection. f, femur; t, tibia. (**f–i**) Inhibition of coronal suture development by the ectopic presence of $FGF9^{WT}$ and $FGF9^{Eks}$. $FGF9^{WT}$ or $FGF9^{Eks}$ beads were implanted onto the coronal suture in E15 mice, and the *Spp1* expression was examined by *in situ* hybridization 24 h after implantation. On the operated sides with $FGF9^{WT}$ (**f**) and $FGF9^{Eks}$ (**h**) bead implants, there was overlap of *Spp1* expression in the frontal and parietal bones, which was not seen on the unoperated sides (**g**,**i**). fb, frontal bone; pb, parietal bone.

tissues. To address this possibility, we first measured FGF9–heparin affinity by heparin affinity chromatography (**Fig. 5a**). $FGF9^{WT}$ was eluted from heparin-conjugated agarose with 1.50 M NaCl as a single peak. In contrast, most $FGF9^{Eks}$ was eluted at 1.38 M NaCl and a small fraction eluted at 1.10 M NaCl.

We next measured the kinetic constants for the $FGF9^{Eks}$–heparin interaction using surface plasmon resonance analysis (**Fig. 5b,c** and **Supplementary Table 1** online). The resulting sensorgrams were used for kinetic parameter determination by globally fitting the experimental data to a 1:1 interaction model. The association rate constant (k_a) of $FGF9^{Eks}$ was slightly greater than that of $FGF9^{WT}$, whereas the dissociation rate constant (k_d) of $FGF9^{Eks}$ was 18-fold greater than that of $FGF9^{WT}$. The dissociation constants (K_D) for $FGF9^{WT}$ and $FGF9^{Eks}$ were 0.71 ± 0.02 nM and 5.24 ± 0.03 nM, respectively, representing an 86% decrease in affinity of the $FGF9^{Eks}$ protein for heparin.

Dimerization of FGF9 confers heparin affinity

The above studies indicate the $Fgf9^{Eks}$ mutation concurrently affects monomer–dimer equilibrium and affinity for heparin. We thus went on to address whether the N143T substitution directly affects the affinity of FGF9 for heparin or whether it directly affects homodimerization and secondarily affects heparin affinity. However, direct biochemical measurements of the affinity of the two species for heparin are not possible because monomeric and dimeric forms of FGF9 are in equilibrium. We therefore analyzed the configuration of heparin-binding domains in monomeric and dimeric FGF9 using molecular-dynamics simulations and calculated the binding free energy between FGF9 and heparin using the molecular mechanics Poisson-Boltzmann/surface area (MM-PBSA) method. It is well known that the binding free energies calculated by this method show good qualitative but not quantitative agreement with experimental observations[27].

To model the heparin binding affinity of FGF9, we carried out molecular-dynamics simulations of 2:2 $FGF9^{WT}$–heparin and 2:2 $FGF9^{Eks}$–heparin complexes based on a 2:2:2 FGF2-FGFR1-heparin crystal structure (Protein Data Bank (PDB) ID: 1FQ9)[28]. The conformations of two heparin oligosaccharides in each complex were influenced by strong electrostatic repulsions, resulting in the exclusion of one heparin oligosaccharide from the complex (data not shown). This analysis suggested that 2:2 FGF9–heparin complexes would be unstable. In contrast, molecular-dynamics simulations of 2:1 $FGF9^{WT}$–heparin, 2:1 $FGF9^{Eks}$–heparin, 1:1 $FGF9^{WT}$–heparin and 1:1 $FGF9^{Eks}$–heparin complexes suggested that these complexes are stable (**Fig. 5d–g**). Molecular-dynamics simulations of dimeric FGF9–heparin complexes did not show a big difference in heparin-binding free energies for 2:1 $FGF9^{WT}$–heparin (dimeric $FGF9^{WT}$–heparin) and 2:1 $FGF9^{Eks}$–heparin (dimeric $FGF9^{Eks}$–heparin) complexes (**Fig. 5d,e**). This is due to the strong interaction between the negatively charged heparin oligosaccharide chain and the array of basic amino acid residues located in the heparin binding site near the groove of the dimer interface in both dimeric complexes. In addition, flexibility of the heparin oligosaccharide chain would help to maintain electrostatic interactions. Similarly, there was little difference in the heparin-binding free energies in 1:1 $FGF9^{WT}$–heparin (monomeric $FGF9^{WT}$–heparin) and 1:1 $FGF9^{Eks}$–heparin (monomeric $FGF9^{Eks}$–heparin) complexes (**Fig. 5f,g**). This is also due to heparin oligosaccharide chain flexibility, the strong negative charge of the heparin oligosaccharide and the presence of several basic amino acid residues in the heparin binding site. Therefore, the *Eks* mutation does not seem to influence the heparin binding affinity of either the dimeric or the monomeric FGF9–heparin complex. Because the heparin-binding free energies for dimeric FGF9 (**Fig. 5d,e**) were smaller than those for monomeric FGF9–heparin for both $FGF9^{WT}$ and $FGF9^{Eks}$ (**Fig. 5f,g**), the reduced binding affinity to heparin of the $FGF9^{Eks}$ protein is most likely due to the shift in the monomer–dimer equilibrium toward the monomer. In summary, the *Eks* mutation primarily affects homodimerization of FGF9 and only secondarily affects heparin affinity.

$FGF9^{Eks}$ is potentially hyperdiffusible in tissues

Heparin–FGF2 interactions have previously been shown to regulate the diffusibility of FGF2 (refs. 26,29). We hypothesized that the diffusibility of $FGF9^{Eks}$ in tissues would be increased because of its lower affinity for heparin, leading to ectopic localization outside of the normal signaling domain and, consequently, ectopic activation of FGFRs. However, this model can only be considered if the following two prerequisites are met: first, *Fgf9* and *Fgfrs* are expressed in the proximity of the prospective elbow and knee joints and coronal sutures and, second, the increased diffusibility of $FGF9^{Eks}$ is dominant over its decreased ability to activate FGFRs.

We first examined the expression of *Fgf9* and *Fgfr1*, *Fgfr2* and *Fgfr3* in the forelimb buds in E10.5 and E11.5 mice. *Fgf9* was expressed in migrating myoblasts, both in $Fgf9^{+/+}$ and $Fgf9^{Eks/Eks}$ mice (**Supplementary Fig. 3a,b,i,j** online). At E10.5, *Fgfr1*, *Fgfr2* and *Fgfr3* were expressed diffusely in the limb bud mesenchyme, overlapping the expression domain of *Col2a1* in both $Fgf9^{+/+}$ and $Fgf9^{Eks/Eks}$ tissues (**Supplementary Fig. 3c–h**). At E11.5, *Fgfr1* expression was excluded from the cartilaginous condensation, whereas *Fgfr2* and *Fgfr3*

expression was observed mainly in this location (**Supplementary Fig. 3k–p**). Therefore, mesenchymal cells in the prospective elbow joint express FGFRs.

Previous reports showed that *Fgf9* is expressed in the developing frontal and parietal bones, particularly strongly at the rims of the bones[18]. *Fgfr1*, *Fgfr2* and *Fgfr3* are expressed within and around the developing frontal and parietal bone domains[30]. Thus, the first prerequisite was validated.

FGF9^{Eks} is able to inhibit joint and suture development

To address the second prerequisite for our model, we examined the inhibitory effects of FGF9^{WT} and FGF9^{Eks} on joint development by ectopically expressing them in the chicken limb bud using a replication component retroviral vector (RCAS) transduction. RCAS-*Fgf9*^{WT}, RCAS-*Fgf9*^{Eks} or empty RCAS virus was used to infect the prospective hindlimb bud region in the lateral plate mesoderm. FGF9^{WT} and FGF9^{Eks} were expressed throughout the hindlimb buds (**Fig. 6a,b**). Ectopic expression of both *Fgf9*^{WT} and *Fgf9*^{Eks} caused knee joint fusion (**Fig. 6c,d**), whereas no abnormalities were induced by the empty vector (**Fig. 6e**). Therefore, FGF9^{Eks} retains inhibitory effects on joint development as well as FGF9^{WT}. It is notable that skeletal defects induced by the expression of FGF9^{WT} were widespread, whereas those mediated by FGF9^{Eks} were limited to the prospective joint regions. This is consistent with our finding that FGF9^{Eks} preferentially activates FGFR3c (**Fig. 4**), which is expressed in the bone anlagen (**Supplementary Fig. 3**), whereas FGF9^{WT} is expected to activate all of the mesodermally expressed FGFRs.

To examine the inhibitory effects of FGF9^{WT} and FGF9^{Eks} on suture development, we implanted FGF9-soaked AffiGel-Blue beads in the coronal suture of normal mouse fetal skulls around the initiation stage of the suture defect, at E15, by *ex utero* surgery. We first confirmed that approximately equal amounts of FGF9^{WT} and FGF9^{Eks} were loaded in each AffiGel-Blue bead and that the diffusion rates of FGF9^{WT} and FGF9^{Eks} from the beads were almost identical (**Supplementary Fig. 4** online). The expression of *Spp1*, an early osteoblast differentiation marker upregulated by FGF9, was examined 24 h after *in utero* bead placement. Grafts of FGF9^{WT} and FGF9^{Eks} beads also promoted ectopic *Spp1* expression at the leading edges of the frontal and parietal bones (**Fig. 6f–i**). This FGF9-induced ectopic expression of *Spp1* resembled that observed in the *Fgf9*$^{Eks/Eks}$ coronal suture (**Fig. 2m**, right). Therefore, ectopic expression of either FGF9^{Eks} or FGF9^{WT} within the suture inhibits suture development.

FGF9^{Eks} is more diffusible than FGF9^{WT} in developing tissues

To examine whether the diffusibility of FGF9^{Eks} in mesenchymal tissue is increased in comparison with FGF9^{WT}, we measured the diffusibility of FGF9^{WT} and FGF9^{Eks} in the skull following bead implantation (**Fig. 7a–e**). Because FGF9 upregulates *Spp1* expression, we could measure the area of high *Spp1* expression as an indication of

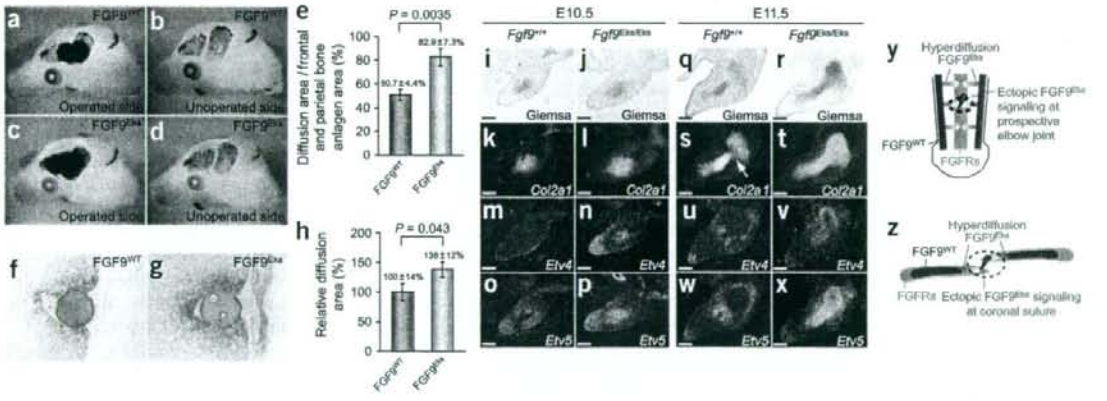

Figure 7 Ectopic FGF9^{Eks} signaling due to its hyperdiffusibility. (**a–e**) Increased diffusibility of FGF9^{Eks} in the skull bone anlagen. FGF9^{WT} or FGF9^{Eks} beads were implanted onto the coronal suture at E15 mice and *Spp1* expression was examined by whole-mount *in situ* hybridization 24 h after implantation. On the operated sides with FGF9^{WT} (**a**) and FGF9^{Eks} (**c**) bead implants, we observed well-defined intense signals in the frontal and parietal bone anlagen around the implants, which were not seen on the unoperated side (**b,d**). This domain with intense *Spp1* signals reflects diffusibility of exogenous FGF9 proteins. We therefore compared diffusibility of FGF9^{WT} and FGF9^{Eks} based on the induced expression domain of *Spp1* (**e**). The diffusion areas (%) in the frontal and parietal bone anlagen area were estimated from the area ratio of the intense *Spp1* expression against the frontal and parietal bone anlagen. Data are represented as mean ± s.e.m. of six operations. FGF9^{Eks} is more diffusible than FGF9^{WT}. Significance was determined by two-tailed Student's *t*-test. (**f–h**) Increased diffusibility of FGF9^{Eks} in the forelimb bud. FGF9^{WT} or FGF9^{Eks} beads were implanted into forelimb buds of *Fgf9*$^{-/-}$ embryos of E10.5 mice. Diffusion of exogenous FGF9^{WT} (**f**) and FGF9^{Eks} (**g**) after 2 h was immunodetected using a FGF9 antibody. (**h**) The diffusion area of FGF9^{Eks} and FGF9^{WT} was measured at the level of the equator of the beads. Data are represented as mean (FGF9^{WT} = 100%) ± s.e.m. of four (FGF9^{WT}) or five (FGF9^{Eks}) operations. FGF9^{Eks} is also more diffusible than FGF9^{WT} in limb buds. Significance was determined by one-tailed Student's *t*-test. (**i–x**) The downstream target genes of FGF signaling, *Etv4* and *Etv5*, are expressed ectopically in the prospective elbow joint in *Fgf9*$^{Eks/Eks}$ mice. Counterstaining with Giemsa (**i,j,q,r**) and *in situ* detection of *Col2a1* (**k,l,s,t**), *Etv4* (**m,n,u,v**) and *Etv5* (**o,p,w,x**) in the forelimb buds of *Fgf9*$^{+/+}$ and *Fgf9*$^{Eks/Eks}$ embryos at E10.5 and E11.5. There was ectopic expression of *Etv4* (**n,v**) and *Etv5* (**p,x**), in the cartilaginous condensation including the prospective elbow joint position, which was demarcated as the gap of *Col2a1* expression (**s**, arrow), in *Fgf9*$^{Eks/Eks}$, which were not seen in *Fgf9*$^{+/+}$ mice (**m,o,u,w**). Scale bars, 100 μm. (**y**) A model for the pathogenic mechanism underlying elbow joint synosotsis in *Fgf9*$^{Eks/Eks}$ mice. In *Fgf9*$^{Eks/Eks}$ mice, ectopic FGF9 signaling due to hyperdiffusion of FGF9^{Eks} at the prospective elbow joint may inhibit the initiation of joint development. (**z**) A model for the pathogenic mechanism underlying premature fusion of the coronal suture in *Fgf9*$^{Eks/Eks}$ mice. In *Fgf9*$^{Eks/Eks}$ mice, ectopic FGF9 signaling due to hyperdiffusion of FGF9^{Eks} at the coronal suture may promote ectopic osteogenesis and subsequently induce premature fusion of the suture.

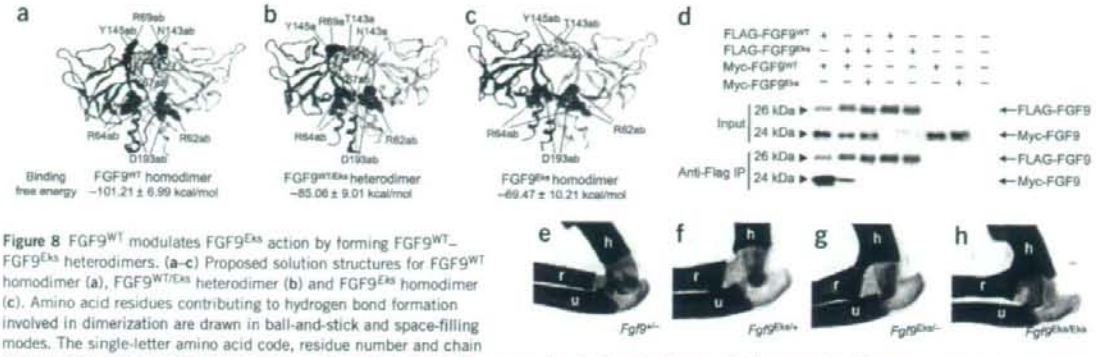

Figure 8 $FGF9^{WT}$ modulates $FGF9^{Eks}$ action by forming $FGF9^{WT}$–$FGF9^{Eks}$ heterodimers. (**a–c**) Proposed solution structures for $FGF9^{WT}$ homodimer (**a**), $FGF9^{WT/Eks}$ heterodimer (**b**) and $FGF9^{Eks}$ homodimer (**c**). Amino acid residues contributing to hydrogen bond formation involved in dimerization are drawn in ball-and-stick and space-filling modes. The single-letter amino acid code, residue number and chain code are indicated for each of these residues. Computed binding free energy of each dimer is shown under the respective illustrated structure. Data are represented as mean ± s.d. of energies obtained from 200 molecular-dynamics snapshots in respective molecular-dynamics trajectory. (**d**) $FGF9^{WT}$ is capable of forming dimers with $FGF9^{Eks}$. The expression of $FGF9^{WT}$ homodimers, $FGF9^{WT/Eks}$ heterodimers and $FGF9^{Eks}$ homodimers was analyzed using immunoprecipitation and protein blots. The expression vectors for FLAG- or Myc-tagged $FGF9^{WT}$ and $FGF9^{Eks}$ were transfected into COS7 cells and culture supernatants were subjected to immunoprecipitation and protein blot analysis. (**e–h**) Less severe elbow joint synostosis in $Fgf9^{Eks/+}$ than $Fgf9^{Eks/-}$. Forelimbs from $Fgf9^{+/-}$, $Fgf9^{Eks/+}$, $Fgf9^{Eks/-}$ and $Fgf9^{Eks/Eks}$ embryos at E17.5 were stained with Alcian blue and Alizarin red. Synostotic change is restricted to the cartilaginous component in $Fgf9^{Eks/+}$ embryos, whereas it is extended to the bony component in $Fgf9^{Eks/-}$ and $Fgf9^{Eks/Eks}$ embryos. h, humerus; r, radius; u, ulna.

the distance over which FGF9 exerts its effects. Implantation of $FGF9^{Eks}$ beads resulted in a larger area of *Spp1* expression (high *Spp1* expression area / Frontal and parietal bone anlagen area = 82.9 ± 7.3%) (± s.e.m.) compared with beads loaded with $FGF9^{WT}$ (50.7 ± 4.4%; $P = 0.0035$), suggesting that the altered protein diffused more effectively through the developing tissue.

Next, we investigated the diffusibility of $FGF9^{Eks}$ in forelimb buds. $FGF9^{WT}$- or $FGF9^{Eks}$-soaked AffiGel-Blue beads were grafted into the dorsal and central forelimb bud region of $Fgf9^{-/-}$ embryos around the initiation stage of the joint defect, at E10.5. FGF9 protein released from the beads into mesenchymal tissue 2 h after implantation was detected by immunohistochemistry using FGF9 antibodies on sections (**Fig. 7f–h**). This analysis showed that $FGF9^{Eks}$ permeated through the limb bud mesenchyme to a greater extent (relative disffusion area = 138 ± 12%) (± s.e.m.) than $FGF9^{WT}$ (100 ± 14%; $P = 0.043$), supporting the hypothesis that $FGF9^{Eks}$ is more diffusible than $FGF9^{WT}$.

Ectopic FGF signaling in the prospective joint of *Eks* mice

To examine whether diffusion of endogenous $FGF9^{Eks}$ is increased in comparison to $FGF9^{WT}$, we determined the degree of activation of FGFRs in the prospective elbow joint of $Fgf9^{Eks/Eks}$ mice. As a readout for FGFR signaling, we examined the expression of *Etv4* and *Etv5*, both of which are known to be transcriptionally activated by FGF signaling, in the forelimb buds[31] (**Fig. 7i–x**). In wild-type E10.5 limbs, we did not observe the intensive expression of *Etv4* or *Etv5* within the region undergoing cartilaginous condensation demarcated by *Col2a1* expression (**Fig. 7m,o**). However, in E10.5 $Fgf9^{Eks/Eks}$ limbs, we found ectopic expression of both *Etv4* and *Etv5* in the cartilaginous condensation (**Fig. 7n,p**). At E11.5, *Etv4* and *Etv5* were expressed in the myoblasts and cells surrounding the cartilaginous condensation in wild-type mice (**Fig. 7u,w**), whereas in $Fgf9^{Eks/Eks}$ mice, we observed clear expression of *Etv4* and *Etv5* in the cartilaginous condensation including the prospective elbow joint position (**Fig. 7v,x**). These results demonstrate ectopic FGF signaling in the prospective elbow joint in $Fgf9^{Eks/Eks}$ mice. Because the ectopic expression domain of *Etv4* and *Etv5* in $Fgf9^{Eks/Eks}$ mice was not consistent with the *Fgf9* expression domain (**Supplementary Fig. 3a,b,i,j**), this outcome is likely due to increased diffusion of $FGF9^{Eks}$ protein over a larger area than $FGF9^{WT}$.

From these results, we propose a mechanism of elbow joint synostosis in $Fgf9^{Eks/Eks}$ mice in which $FGF9^{Eks}$ produced by myoblasts diffuses beyond its normal range and ectopically activates FGFRs in the prospective elbow joint, preventing joint formation (**Fig. 7y**). Similarly, $FGF9^{Eks}$ produced at the rims of the frontal and parietal bones diffuses beyond its normal area and ectopically activates FGFRs in the coronal suture mesenchyme, promoting the fusion of coronal sutures (**Fig. 7z**).

Genetic validation of the hyperdiffusible model

A prediction of our model is that the severity of synostotic phenotypes will correlate with a shift in the equilibrium of FGF9 from dimer toward monomer. By molecular-dynamics simulations, we estimated that $FGF9^{WT}$ homodimer, $FGF9^{WT/Eks}$ heterodimer and $FGF9^{Eks}$ homodimer have ten, eight, six intermonomer hydrogen bonds, respectively (**Fig. 8a–c** and **Supplementary Table 2** online). From these results, we calculated the binding free energy of the $FGF9^{WT/Eks}$ heterodimer to be between those of the $FGF9^{WT}$ and $FGF9^{Eks}$ homodimers (**Fig. 8a–c**), suggesting that $FGF9^{WT/Eks}$ heterodimers are more stable than $FGF9^{Eks}$ homodimers. If our model is correct, $FGF9^{WT}$ should interfere with $FGF9^{Eks}$ action by forming $FGF9^{WT/Eks}$ heterodimers. In other words, skeletal phenotypes due to the *Eks* mutation should be alleviated by the expression of $FGF9^{WT}$.

We first sought experimental evidence that the $FGF9^{WT/Eks}$ heterodimer was substantially more stable than the $FGF9^{Eks}$ homodimer. We addressed this issue by immunoprecipitation and protein blot analysis after tagging $FGF9^{WT}$ and $FGF9^{Eks}$ with Flag or Myc peptides. Flag-$FGF9^{WT}$ or Flag-$FGF9^{Eks}$ was overexpressed together with Myc-$FGF9^{WT}$ or Myc-$FGF9^{Eks}$ in COS7 cells and the culture supernatants were subjected to the immunoprecipitation and protein blot analysis (**Fig. 8d**). We readily detected Flag-$FGF9^{WT}$–Myc-$FGF9^{WT}$ dimers. Flag-$FGF9^{Eks}$–Myc-$FGF9^{WT}$ dimers were detected at lower level; however, Flag-$FGF9^{Eks}$–Myc-$FGF9^{Eks}$

dimers did not form under these conditions. These data suggest that $FGF9^{WT}$ and $FGF9^{Eks}$ can form heterodimers that are more stable than $FGF9^{Eks}$ homodimers.

We finally examined whether the elbow synostosis caused by $FGF9^{Eks}$ could be alleviated by the expression of $FGF9^{WT}$. We thus compared the severity of elbow synostosis in $Fgf9^{Eks/+}$ and compound heterozygous mutants ($Fgf9^{Eks/-}$) relative to that of $Fgf9^{+/-}$ and $Fgf9^{Eks/Eks}$ mice (**Fig. 8e–h**). Elbow joint formation was not affected in $Fgf9^{+/-}$ mice (**Fig. 8e**), whereas elbow synostosis in $Fgf9^{Eks/Eks}$ mice involved both cartilaginous and bony components (**Fig. 8h**). In contrast, the synostosis in $Fgf9^{Eks/+}$ mice was limited to the cartilaginous component (**Fig. 8f**), whereas the involvement of the bony component in $Fgf9^{Eks/-}$ mice was similar to that of $Fgf9^{Eks/Eks}$ mice (**Fig. 8g**). Therefore, elbow synostosis in $Fgf9^{Eks/-}$ is more severe than in $Fgf9^{Eks/+}$. These findings strongly support our model that the monomer–dimer status of FGF9 influences its affinity for HSPGs and, consequently, its distribution in developing tissues.

DISCUSSION

In the present study, we identified a missense mutation in the *Fgf9* gene that is responsible for the *Eks* mutant phenotype, which includes elbow and knee joint synostosis and craniosynostosis. We further demonstrate that the N143T substitution in FGF9 favors formation of the monomeric form of FGF9, which binds to heparin with a lower affinity than dimeric FGF9. The decreased affinity for heparin leads to increased diffusion of the altered protein in developing tissues, resulting in ectopic FGF9 signaling. We propose that regulation of the monomer–dimer equilibrium of FGF9, and potentially of other FGFs, and its affinity for HSPGs is a mechanism that functions to shape FGF9 concentration gradients in developing tissues. We further propose that these biochemical properties of FGF9 restrict its signaling activity to limited skeletal domains. Data presented here and in previous studies indicate that low FGF signaling in the presumptive joint space is necessary for the formation of the joint space and maintenance of an open suture[20,21]. Common usage of receptor binding and homodimerization sites of FGF9 could be at least in part instrumental for local modulation of FGF9 signaling activity.

Homodimerization is suggested to be a common feature of the FGF9/16/20 subfamily[32] and of FGF2 (refs. 33,34). It is not known to what extent homodimerization affects the activity of other FGFs. The discovery that a mutation in *Fgf9* can affect homodimerization, affinity for heparin and biological activity suggests that pharmacological agents that affect FGF homodimerization could be useful tools to modulate its activity.

METHODS

Detection of a mutation in the *Fgf9* gene. To identify the mutation responsible for the *Eks* mutant phenotype, we surveyed the cDNA sequence of *Fgf9* from normal (+/+), heterozygous (*Eks*/+) and homozygous (*Eks*/*Eks*) mice through reverse transcription-PCR (RT-PCR) and direct sequencing of RT-PCR products.

For genotyping of the *Eks* allele, genomic DNA spanning the *Eks* mutation was amplified by PCR using specific primers (**Supplementary Table 3** online). PCR products were digested with the diagnostic *Bsr*I restriction enzyme. Wild-type mice show two bands of 147 bp and 42 bp, whereas the *Eks* allele shows one band of 189 bp (**Supplementary Fig. 5** online).

Skeletal and histological preparations. Bones and cartilage of E17.5 fetuses were stained with Alizarin red and Alcian blue as previously described[35]. For histological preparations, tissues were fixed in 4% paraformaldehyde, embedded in paraffin, sectioned at 5 μm, and stained with hematoxylin and eosin and von Kossa.

***In situ* hybridization.** *In situ* hybridization of paraffin sections was done as previously described[36], using radiolabeled antisense RNA for *Gdf5* (MGI: 95688), *Col2a1* (MGI: 88452), *Spp1* (MGI: 98389), *Runx2* (MGI: 99829), *Fgf9* (MGI: 104723), *Fgfr1* (MGI: 95522), *Fgfr2* (MGI: 95523), *Fgfr3* (MGI: 95524), *Etv4* (MGI: 99423) and *Etv5* (MGI: 1096867). *In situ* hybridization after bead implantation in fetal skulls was done as previously described[24].

$FGF9^{WT}$ and $FGF9^{Eks}$ expression and purification. $FGF9^{WT}$ and $FGF9^{Eks}$ expression and purification were done as described in **Supplementary Methods**.

Analytical ultracentrifugation. All analytical ultracentrifuge experiments were done on a Beckman Coulter XL-I analytical ultracentrifuge. We diluted the samples in 25 mM ammonium acetate buffer (pH 5.5) containing 120 mM NaCl. The partial specific volumes were estimated as 0.7317 ml/g ($FGF9^{WT}$) or 0.7322 ml/g ($FGF9^{Eks}$) by SEDNTERP software. All experiments were done at 20 °C and the absorbance wavelength was 280 nm. We carried out sedimentation equilibrium experiments with six channel centerpieces, with loading concentrations of 0.8, 0.4 and 0.2 mg/ml. Data were obtained at 12, 14 and 16 k rpm for $FGF9^{WT}$ or at 14, 16 and 18 k rpm for $FGF9^{Eks}$. A total equilibration time of 16 h was used for each speed with scans taken at 12, 14 and 16 h. We analyzed the sedimentation equilibrium data using the Beckman XL-A/XL-I Data Analysis software. All nine datasets (three speeds, three concentrations) were fitted together by 'self association model' calculation. Sedimentation velocity experiments were carried out with double sector centerpieces. Protein concentrations were 0.4, 0.3 or 0.2 mg/ml. We scanned the absorbance data 100 times every 5 min at 40 k rpm. The measurements data were analyzed by SEDFIT software.

Analytical gel filtration chromatography. Purified $FGF9^{WT}$ and $FGF9^{Eks}$ (100 μl of 2 mg/ml) were loaded onto a Superdex75 10/300 GL column (GE Healthcare) equilibrated with a 25 mM ammonium acetate buffer (pH 5.5) containing 120 mM NaCl. The samples were eluted with the same buffer.

Mitogenic assays. The ability of $FGF9^{WT}$ and $FGF9^{Eks}$ to transduce signals via FGFRs was analyzed by a mitogenic assay using BaF3 cells expressing specific FGFRs as described previously[17]. We plated 5,000 cells per well in a 96-well assay plate in media containing varying concentrations of FGF9 and heparin (Wako). $FGF9^{WT}$ or $FGF9^{Eks}$ were added to each well for a total volume of 200 μl per well. The cells were then incubated at 37 °C for 36 h. We added 1 μCi of [^{3}H]thymidine to each well in 20 μl of media. The cells were harvested after 4 h by filtration through glass fiber paper and the incorporated [^{3}H]thymidine was counted on a Wallac MicroBeta TriLux scintillation counter (PerkinElmer).

Analytical heparin affinity chromatography. We loaded 3 mg of purified $FGF9^{WT}$ and $FGF9^{Eks}$ onto a 1 ml HiTrap heparin HP column (GE Healthcare) equilibrated with 25 mM ammonium acetate buffer (pH 5.5) containing 120 mM NaCl. The bound $FGF9^{WT}$ or $FGF9^{Eks}$ were eluted with a linear gradient of NaCl (120 mM to 2.0 M) in the same buffer.

Surface plasmon resonance analysis of FGF9–heparin interactions. Surface plasmon resonance analysis for measurements of $FGF9^{WT}$–heparin and $FGF9^{Eks}$–heparin interactions were done using a BIAcore 3000 instrument (Biacore AB). In order to immobilize heparin (Wako) on the streptavidin-conjugated sensor chip SA, 100 μg/ml biotinylated heparin in HBS-EP buffer was injected at a flow rate of 10 μl/min and was immobilized to 63 response units (RU). All measurements were carried out at room temperature, and refractive index errors due to bulk solvent effects were corrected by subtracting responses on the noncoated sensor chip for the $FGF9^{WT}$ and $FGF9^{Eks}$ concentrations used. To obtain kinetic data, we injected different concentrations of analytes ($FGF9^{WT}$ and $FGF9^{Eks}$) in HBS-EP over the heparin sensor chip at a flow rate of 20 μl/min. At the end of each sample injection (120 s), HBS-EP buffer was passed over the sensor surface to monitor the dissociation phase. Following 120 s of dissociation, the sensor surface was regenerated by injection of 5 μl of 1 M NaCl in HBS-EP. We used five different analyte concentrations to determine the kinetic parameters for each interaction. Kinetic parameters were obtained by global fitting of the sensorgrams to a 1:1 model using BIAevaluation software.

Molecular-dynamics simulation. Starting structures of monomeric $FGF9^{WT}$, dimeric $FGF9^{WT}$, monomeric $FGF9^{WT}$-heparin, dimeric $FGF9^{WT}$-heparin and $FGF9^{Eks}$ for molecular-dynamics simulations were taken from the PDB (PDB ID: 1IHK)[14]. The structures of monomeric $FGF9^{Eks}$, dimeric $FGF9^{Eks}$ and heterodimeric $FGF9^{WT/Eks}$ were constructed based on $FGF9^{WT}$ using molecular modeling software MOE (Chemical Computing Group). A hexasasaccharide (UAP-SGN-IDU-SGN-IDU-SGN) is used as a heparin oligosaccharide. UAP is 1,4-dideoxy-5-dehydro-O2-sulfo-glucuronic acid, SGN is O6-disulfo-glucosamin and IDU is 1,4-dideoxy-O2-sulfo-glucuronic acid. For monomeric $FGF9^{WT}$–heparin and dimeric $FGF9^{WT}$–heparin simulations, heparin oligosaccharide was bound to $FGF9^{WT}$ structures obtained from molecular-dynamics simulations using the molecular docking program GOLD (version 3.0)[37]. In the docking protocol, the standard default setting of GA parameters was used and GoldScore was used as the scoring function. The structures of monomeric $FGF9^{Eks}$–heparin and dimeric $FGF9^{Eks}$–heparin were built in the same manner as $FGF9^{WT}$–heparin complexes. All the starting structures for molecular-dynamics simulations were surrounded by TIP3P water molecules[38] spherically. After energy minimizations, all molecular-dynamics simulations were carried out for 10 ns at 300 K using modified Amber 8.0 (ref. 39) for MDGRAPE3 system[40]. The Amber ff03 force field[41] was adopted, and the simulation time step was set at 1 s. We calculated the binding free energies by the molecular mechanics Poisson-Boltzmann/surface area (MM-PBSA) method[42] using the last 2 ns molecular-dynamics trajectories.

Retroviral misexpression. Mouse *Fgf9*^{WT} and *Fgf9*^{Eks} cDNAs were cloned into the RCASBP(A) vector[43]. The virus solutions were injected into the hind limb bud of chicken embryos at Hamburger-Hamilton stage 17. We examined the expression of mouse *Fgf9* transcripts and skeletal changes 2 and 5 d after injection, respectively.

Subcutaneous insertion of $FGF9^{Eks}$ beads in mouse fetal skulls. AffiGel-Blue beads (BioRad) soaked in 100 μg/ml $FGF9^{WT}$ or $FGF9^{Eks}$ were implanted onto E15 mouse skulls by *ex utero* surgery as previously described[24] Operated heads were collected 24 h later and *Spp1* transcripts were detected by whole-mount *in situ* hybridization. The area of *Spp1* expression was measured using NIH image software.

Implantation of $FGF9^{Eks}$ beads in mouse forelimb buds. AffiGel-Blue beads that had been soaked in 500 μg/ml $FGF9^{WT}$ or $FGF9^{Eks}$ were implanted into the dorsal and central region of E10.5 *Fgf9*$^{-/-}$ forelimb buds. Limb buds were subsequently cultured for 2 h on Transwell filters (Costar, Coaning) in serum-free medium (BGJb, 2 mg/ml BSA, penicillin (50 units/ml), streptomycin (50 μg/ml)), in a humid, 37 °C and 5% CO_2 environment. Explants were fixed in 4% paraformaldehyde and embedded in paraffin. Sections through the equator of the bead were analyzed for exogenous FGF9 using goat antibody to FGF9 (R&D Systems) and a cell and tissue staining kit HRP-AEC system (R&D Systems). We analyzed the signal area and intensity using NIH image software.

Immunoprecipitation and protein blot analysis. cDNA fragments encoding the full length mouse $FGF9^{WT}$ and $FGF9^{Eks}$ proteins were cloned into the p3xFlag-CMV-14 vector (Sigma-Aldrich) and into the pCMV-Tag3B vector (Stratagene) to allow expression of FGF9 proteins with either C-terminal Myc or 3xFlag tags. These vectors were transfected into COS7 cells, and 48 h later, culture supernatants were incubated with anti-Flag M2 affinity beads (Sigma-Aldrich) for 1 h at RT and washed three times with PBS and then subjected to protein blots with antibody to Flag M2 (Sigma-Aldrich) or antibody to Myc (Upstate).

Note: Supplementary information is available on the Nature Genetics website.

ACKNOWLEDGMENTS

This study was supported in part by the RIKEN Structural Genomics/Proteomics Initiative (RSGI) and the National Project on Protein Structural and Functional Analysis, Ministry of Education, Culture, Sports, Science and Technology of Japan (S.Y.) and US National Institutes of Health grant HD049808 (D.M.O.).

AUTHOR CONTRIBUTIONS

M.H., D.M.O. and H.K. developed the project and wrote the manuscript. M.H., S.H. and H.K. contributed to the purification of FGF9 proteins, mitogenic assays, analytical gel filtration chromatography, analytical heparin affinity chromatography, surface plasmon resonance analysis, skeletal preparation, histological analyses and *in situ* hybridization of sections, implantation of FGF9 beads in mouse forelimb buds and immunoprecipitation and protein blot analysis. H.M., A.O. and H.K. contributed to the identification of the *Eks* mutation. N.O., N.F. and M.T. contributed to the molecular-dynamics simulation. T.N. and S.I. contributed to the implantation of FGF9 beads in mouse fetal skulls. R.A., M.S. and S.Y. contributed to the analytical ultracentrifugation. Y.S. and A.K. contributed to the retroviral misexpression. Y.M.-K. contributed to the *in situ* hybridization of sections.

Published online at http://www.nature.com/naturegenetics/
Reprints and permissions information is available online at http://npg.nature.com/reprintsandpermissions/

1. Ornitz, D.M. & Itoh, N. Fibroblast growth factors. *Genome Biol.* **2**, reviews 3005 (2001).
2. Wilkie, A.O.M. Bad bone, absent smell, selfish testes: the pleiotropic consequences of human FGF receptor mutations. *Cytokine Growth Factor Rev.* **16**, 187–203 (2005).
3. Su, N., Du, X. & Chen, L. FGF signaling: its role in bone development and human skeleton diseases. *Front. Biosci.* **13**, 2842–2865 (2008).
4. Ornitz, D.M. & Marie, P.J. FGF signaling pathways in endochondral and intramembranous bone development and human genetic disease. *Genes Dev.* **16**, 1446–1465 (2002).
5. Martin, G.R. The roles of FGFs in the early development of vertebrate limbs. *Genes Dev.* **12**, 1571–1586 (1998).
6. Ornitz, D.M. FGF signaling in the developing endochondral skeleton. *Cytokine Growth Factor Rev.* **16**, 205–213 (2005).
7. Montero, A. *et al.* Disruption of the fibroblast growth factor-2 gene results in decreased bone mass and bone formation. *J. Clin. Invest.* **105**, 1085–1093 (2000).
8. Hung, I.H., Yu, K., Lavine, K.J. & Ornitz, D.M. FGF9 regulates early hypertrophic chondrocyte differentiation and skeketal vascularization in the developing stylopod. *Dev. Biol.* **307**, 300–313 (2007).
9. Liu, Z., Xu, J., Colvin, J.S. & Ornitz, D.M. Coordination of chondrogenesis and osteogenesis by fibroblast growth factor 18. *Genes Dev.* **16**, 859–869 (2002).
10. Ohbayashi, N. *et al.* FGF18 is required for normal cell proliferation and differentiation during osteogenesis and chondrogenesis. *Genes Dev.* **16**, 870–879 (2002).
11. Garofalo, S. *et al.* Skeletal dysplasia and defective chondrocyte differentiation by targeted overexpression of fibroblast growth factor 9 in transgenic mice. *J. Bone Miner. Res.* **14**, 1909–1915 (1999).
12. Ornitz, D.M. FGFs, heparan sulfate and FGFRs: complex interactions essential for development. *Bioessays* **22**, 108–112 (2000).
13. Nybakken, K. & Perrimon, N. Heparan sulfate proteoglycan modulation of developmental signaling in *Drosophila*. *Biochim. Biophys. Acta* **1573**, 280–291 (2002).
14. Plotnikov, A.N. *et al.* Crystal structure of fibroblast growth factor 9 reveals regions implicated in dimerization and autoinhibition. *J. Biol. Chem.* **276**, 4322–4329 (2001).
15. Hecht, H.J. *et al.* Structure of fibroblast growth factor 9 shows a symmetric dimer with unique receptor- and heparin-binding interfaces. *Acta Crystallogr. D Biol. Crystallogr.* **57**, 378–384 (2001).
16. Murakami, H. *et al.* Elbow knee synostosis (Eks): a new mutation on mouse Chromosome 14. *Mamm. Genome* **13**, 341–344 (2002).
17. Ornitz, D.M. *et al.* Receptor specificity of the fibroblast growth factor family. *J. Biol. Chem.* **271**, 15292–15297 (1996).
18. Hajihosseini, M.K. & Heath, J.K. Expression patterns of fibroblast growth factors-18 and -20 in mouse embryos is suggestive of novel roles in calvarial and limb development. *Mech. Dev.* **113**, 79–83 (2002).
19. Colvin, J.S., Feldman, B., Nadeau, J.H., Goldfarb, M. & Ornitz, D.M. Genomic organization and embryonic expression of the mouse fibroblast growth factor 9 gene. *Dev. Dyn.* **216**, 72–88 (1999).
20. Wang, Q., Green, R.P., Zhao, G. & Ornitz, D.M. Differential regulation of endochondral bone growth and joint development by FGFR1 and FGFR3 tyrosine kinase domains. *Development* **128**, 3867–3876 (2001).
21. Eswarakumar, V.P., Horowitz, M.C., Locklin, R., Morriss-Kay, G.M. & Lonai, P. A gain-of-function mutation of *Fgfr2c* demonstrates the roles of this receptor variant in osteogenesis. *Proc. Natl. Acad. Sci. USA* **101**, 12555–12560 (2004).
22. Storm, E.E. & Kingsley, D.M. Joint patterning defects caused by single and double mutations in members of the bone morphogenetic protein (BMP) family. *Development* **122**, 3969–3979 (1996).
23. Nalin, A.M., Greenlee, T.K. & Sandell, L.J. Collagen gene expression during development of avian synovial joints: Transient expression of types II and XI collagen genes in the joint capsule. *Dev. Dyn.* **203**, 352–362 (1995).
24. Iseki, S. *et al. Fgfr2* and *osteopontin* domains in the developing skull vault are mutually exclusive and can be altered by locally applied FGF2. *Development* **124**, 3375–3384 (1997).

25. Yoshida, T. *et al.* Twist is required for establishment of the mouse coronal suture. *J. Anat.* **206**, 437–444 (2005).
26. Flaumenhaft, R., Moscatelli, D. & Rifkin, D.B. Heparin and heparan sulfate increase the radius of diffusion and action of basic fibroblast growth factor. *J. Cell Biol.* **111**, 1651–1659 (1990).
27. Woo, H.J. & Roux, B. Calculation of absolute protein-ligand binding free energy from computer simulations. *Proc. Natl. Acad. Sci. USA* **102**, 6825–6830 (2005).
28. Schlessinger, J. *et al.* Crystal structure of a ternary FGF-FGFR-heparin complex reveals a dual role for heparin in FGFR binding and dimerization. *Mol. Cell* **6**, 743–750 (2000).
29. Dowd, C.J., Cooney, C.L. & Nugent, M.A. Heparan sulfate mediates bFGF transport through basement membrane by diffusion with rapid reversible binding. *J. Biol. Chem.* **274**, 5236–5244 (1999).
30. Johnson, D., Iseki, S., Wilkie, A.O.M. & Morriss-Kay, G.M. Expression patterns of Twist and *Fgfr1*, *-2* and *-3* in the developing mouse coronal suture suggest a key role for Twist in suture initiation and biogenesis. *Mech. Dev.* **91**, 341–345 (2000).
31. Tsang, M. & Dawid, I.B. Promotion and attenuation of FGF signaling through the Ras-MAPK pathway. *Sci. STKE* **2004**, pe17 (2004).
32. Mohammadi, M., Olsen, S.K. & Ibrahimi, O.A. Structural basis for fibroblast growth factor receptor activation. *Cytokine Growth Factor Rev.* **16**, 107–137 (2005).
33. Ornitz, D.M. *et al.* Heparin is required for cell-free binding of basic fibroblast growth factor to a soluble receptor and for mitogenesis in whole cells. *Mol. Cell. Biol.* **12**, 240–247 (1992).
34. Venkataraman, G., Shriver, Z., Davis, J.C. & Sasisekharan, R. Fibroblast growth factors 1 and 2 are distinct in oligomerization in the presence of heparin-like glycosaminoglycans. *Proc. Natl. Acad. Sci. USA* **96**, 1892–1897 (1999).
35. Kessel, M. & Gruss, P. Murine developmental control genes. *Science* **249**, 374–379 (1990).
36. Kessel, M. & Gruss, P. Homeotic transformations of murine vertebrae and concomitant alteration of Hox codes induced by retinoic acid. *Cell* **67**, 89–104 (1991).
37. Verdonk, M.L., Cole, J.C., Hartshorn, M.J., Murray, C.W. & Taylor, R.D. Improved protein-ligand docking using GOLD. *Proteins* **52**, 609–623 (2003).
38. Jorgensen, W.L., Chandrasekhar, J., Madura, J.D., Impey, R.W. & Klein, M.L. Comparison of simple potential functions for simulating liquid water. *J. Chem. Phys.* **79**, 926–935 (1983).
39. Case, D.A. *et al. AMBER 8* (University of California, San Francisco, 2004).
40. Narumi, T. *et al.* A 55 Tflops simulation of amyloid-forming peptides from yeast prion Sup35 with the special-purpose computer System MD-GRAPE3. <http://doi.acm.org/10.1145/1188455.1188506> (2006).
41. Duan, Y. *et al.* A point-charge force field for molecular mechanics simulations of proteins based on condensed-phase quantum mechanical calculations. *J. Comput. Chem.* **24**, 1999–2012 (2003).
42. Srinivasan, J., Miller, J., Kollma, P.A. & Case, D.A. Continuum solvent studies of the stability of RNA hairpin loops and helices. *J. Biomol. Struct. Dyn.* **16**, 671–682 (1998).
43. Hughes, S.H., Greenhouse, J.J., Petropoulos, C.J. & Sutrave, P. Adaptor plasmids simplify the insertion of foreign DNA into helper-independent retroviral vectors. *J. Virol.* **61**, 3004–3012 (1987).